URSI GASS 2021, Rome, Italy, 28 August - 4 September 2021

Link Budget Analysis for the Modeling of GNSS-R Sea Surface Returns in Far-from-Specular Acquisition Geometries

Gerardo Di Martino, Alessio Di Simone*, Giorgio Franceschetti, Antonio Iodice, Daniele Riccio, and Giuseppe Ruello
Department of Information Technology and Electrical Engineering, University of Naples Federico II, 80125 Naples, Italy

Abstract

For the analysis of sea surface using Global Navigation Satellite System-Reflectometry (GNSS-R), Geometrical Optics (GO) is typically adopted for modeling scattering around the specular reflection direction, where conventional GNSS-R receivers operate. However, the exploitation of GNSS-R for maritime surveillance applications, e.g., ship detection, is feasible in far-from-specular acquisition geometries, where the validity of GO is questionable. In this paper, we present the results of a link budget analysis for the sea surface return in arbitrary viewing geometries. The study is aimed at comparing GO with a more accurate closed-form bistatic two-scale model, named BA-PTSM, for the simulation of GNSS-R signals in acquisition geometries other than the conventional forward-scattering one. Numerical results show that a reliable simulation of airborne GNSS-R signals in far-from-specular acquisition geometries requires sea surface scattering models more accurate than GO, e.g., BA-PTSM.

1 Introduction

In remote sensing applications over oceans, Global Navigation Satellite System-Reflectometry (GNSS-R) has been successfully exploited for the retrieval of key geophysical parameters such as wind speed, sea surface roughness, ocean altimetry [1]. For sea surface analysis, GNSS-R instruments typically operate in a forward-scattering configuration, where the receiver (either airborne or spaceborne) collects the GNSS signal scattered off a portion of sea surface surrounding the specular reflection point, the so-called *glistening zone* [1].

More recently, GNSS-R has been explored for near real-time ship detection/tracking at open sea [2], [3]. Most interesting features of GNSS-R for maritime surveillance applications are the global and seamless coverage of Earth' surface as well as the availability of 100+ GNSS transmitters at no cost. However, a fruitful exploitation of GNSS-R data for ship detection applications is a challenging task due to the very low signal-to-noise ratio (SNR) of the received signal. The feasibility of detecting ship targets using GNSS-R data has been the subject of different theoretical analyses [4], [5], [6]. All such works agree that the conventional forward-scattering GNSS-R operational mode, which is suited to sea surface analysis, is scarcely adapted to intercept the signal scattered from ship targets. To this end, acquisition geometries close to backscattering are definitely preferred. This has been recently demonstrated in a simulation study based on a stochastic simulation of the delay-Doppler map (DDM) and on an analytical scattering model for the ship target [7]. Within GNSS-R literature, scattering from sea surface is described via Geometrical Optics (GO), whose applicability is questionable in directions which are far enough from the specular one. As a matter of fact, an accurate evaluation of sea surface scattering in arbitrary acquisition geometries (also including backscattering) might require more reliable models.

In this paper, we rely on our recent bistatic anisotropic polarimetric two-scale model (BA-PTSM) for the description of sea surface scattering [8]. BA-PTSM is an analytical model which extends the backscattering polarimetric two-scale model (PTSM) presented in [9] to bistatic geometries and to anisotropic rough surfaces.

In order to provide an accurate link budget analysis of the GNSS signal scattered off the sea surface, a numerical evaluation of the scattering area is performed as well taking into account the acquisition geometry, the receiver processing scheme and the antenna beam. Such an analysis might be fruitfully exploited for the simulation of GNSS signals scattered off sea surface in far-from-specular geometries.

2 Bistatic Sea Surface Scattering Model

The two-scale model (TSM) was first introduced in [10] to describe the backscattering from rough surfaces. TSM is based on the concept of composite surface, which is a surface that can be expressed as the superposition of two terms: a small-scale roughness with horizontal scale of the order of wavelength and vertical deviations much smaller than wavelength; a large-scale roughness with horizontal scale very large compared to wavelength and vertical deviations of the order of wavelength or higher. Consequently, the scattering surface is described as a collection of patches whose roughness is the small-scale roughness and tilted randomly according to the large-scale roughness. The Small Perturbation Method (SPM) and GO are adopted to evaluate scattering from the small-scale and large-scale roughness components, respectively. Accordingly, for scattering evaluation, the small-scale roughness is described via its power spectral density (PSD) and dominates scattering in far-from-specular directions, while the large-scale roughness is completely characterized by the probability density function of the

local slopes and mainly contributes to the field scattered around the specular direction.

Unfortunately, TSM allows a closed-form expression of only the co-polarized scattering coefficients, the remaining elements of the covariance matrix requiring numerical evaluation of four-fold integrals. A closed-form polarimetric version of TSM, named PTSM, was presented in [9], where analytical expressions of the whole covariance matrix in backscattering were provided. As opposed to TSM, PTSM allows for a fast evaluation of both cross-polarization and de-polarization effects. Further generalizations of the PTSM to anisotropic rough surfaces (A-PTSM), e.g., sea surface, and bistatic geometries (BA-PTSM) have been carried out in [11] and [8], respectively.

According to BA-PTSM, the PSD of the facet is described through the high-frequency region of the Elfouhaily spectrum, whereas the local slopes of the large-scale roughness, s_x and s_y, are modeled as zero-mean jointly Gaussian random variables. Both the PSD and local slopes statistics depend on the wind speed and direction [8].

In BA-PTSM, the elements of the scattering covariance matrix $R_{pq,rs}$ are expressed as [8]-[9], [11]

$$R_{pq,rs} = R_{pq,rs}^{GO} + \langle R_{pq,rs}^{SPM} \rangle_{s_x,s_y} \quad (1)$$

where the subscripts *p, q, r*, and *s* may each stand for horizontal and vertical polarization and $\langle \cdot \rangle_{s_x,s_y}$ denotes the statistical mean with respect to the large-scale local slopes. In (1), $R_{pq,rs}^{GO}$ is the scattering contribution of the large-scale roughness evaluated through GO, while $R_{pq,rs}^{SPM}$ is the SPM contribution from the tilted rough facet evaluated via a second-order power-series expansion around zero slopes.

Finally, in [8] a basis change is performed in order to get the covariance matrix in the circular polarization channels, which are of interest in GNSS-R.

BA-PTSM reduces to GO around the specular direction but is much more accurate than GO in the other directions. As a matter of fact, BA-PTSM exhibits much wider validity limits compared to GO and offers an accuracy similar to advanced numerical models such as second-order small-slope approximation (SSA2), with the advantage of a much lower computational burden [8].

3 Link Budget for GNSS-R Sea Surface Returns

Here we are interested in evaluating the SNR of the sea surface returns at the output of the standard GNSS-R processing, which includes both a coherent and an incoherent integration step. The final outcome of this processing scheme is the DDM. To this end, the received signal strength at the output of the GNSS-R receiver can be expressed as

$$P_{r,sea} = P_t G_t G_r \frac{1}{(4\pi)^3} \left(\frac{\lambda cos\vartheta cos\vartheta_s}{h_t h_r} \right)^2 A_{sea} \sigma_{sea}^0 , \quad (2)$$

where the normalized radar cross section (NRCS) of sea surface is evaluated via BA-PTSM, which takes as input viewing geometry parameters –viewing and scattering angles–, sensors parameters –radar frequency, polarization–, and scene parameters –dielectric constant (complex) of seawater, wind speed U_{10} and wind direction φ_w. Parameters appearing in (2) are defined in Table I.

Noise power at the output of the receiver front-end is proportional to the receiver bandwidth and is evaluated as

$$P_n = k_B (T_a + T_e) B_W \ . \quad (3)$$

SNR is here evaluated at the output of the incoherent integration step as follows

$$SNR = B_W T_c \sqrt{\frac{T_i}{T_c}} \frac{P_{r,sea}}{P_n} \ . \quad (4)$$

In (3) k_B is the Boltzmann constant, while remaining parameters appearing in (3) and (4) are defined in Table I, where values are reported for Global Positioning System and considering SGR-ReSi and GOLD-RTR as the spaceborne and airborne GNSS-R receivers, respectively [6]. The coordinate system used for defining the viewing and scattering angles is shown in Fig. 1. In this geometry, the specular direction (or forward-scattering) is identified by $\vartheta_s = \vartheta$ and $\varphi_s = 0°$, while backscattering corresponds to $\vartheta_s = \vartheta$ and $\varphi_s = 180°$.

TABLE I: LIST OF SYMBOLS AND VALUES.

Symbol	Parameter	Value
P_t	Transmitted power	26.61 W
G_t	Transmitting antenna gain	13 dBi
G_r	Receiving antenna gain	13.3 dBi (spaceborne) 15.05 dBi (airborne)
λ	GNSS wavelength	0.19 m
ϑ	Viewing angle	Varying
ϑ_s	Zenith scattering angle	Varying
h_t	Transmitter altitude	20200 km
h_r	Receiver altitude	540 km (spaceborne) 10 km (airborne)
A_{sea}	Scattering area	Varying
σ_{sea}^0	Sea scattering coefficient	Evaluated according to [8]
T_a	Receiving antenna noise temperature	99.4 K
T_e	Receiver noise temperature	374.35 K (spaceborne) 161.23 K (airborne)
B_W	Receiver bandwidth	2.5 MHz (spaceborne) 24 MHz (airborne)
T_i	Incoherent integration time	1 s
T_c	Coherent integration time	1 ms (spaceborne) 10 ms (airborne)
τ_c	Chip length	977.52 ns

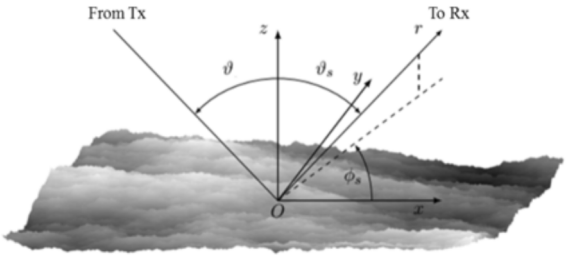

Figure 1: Cartesian reference system and angles definition.

Finally, in (4), the term $B_W T_c$ is the coherent integration gain, while T_i/T_c is equal to the number of DDMs which are incoherently integrated and, then, its square root represents the incoherent integration gain.

4 Numerical Results

In this section, we present numerical results of the SNR of the sea surface returns evaluated according to (2)-(4) assuming the parameters values reported in Table I. The scattering area A_{sea} is computed by means of a simulator of the GNSS-R geometry that takes into account the relative position of the transmitter, the scatterer and the receiver and the receiving antenna beamwidth. The algorithm comprises two steps: first, given the widths of the Woodward Ambiguity Function along the delay and Doppler axes, i.e., $\Delta\tau = 2\tau_c$ and $\Delta f_d = 2/T_c$, respectively, the GNSS-R resolution cell in the delay-Doppler domain $A_{cell} = \Delta\tau\Delta f_d$ is projected onto the Earth-centered Earth-fixed coordinate system. Then, the projected resolution cell is intersected with the receiving antenna footprint to give the scattering area A_{sea}. This latter step is crucial for the airborne configuration, as in this case the receiving antenna footprint might not cover the whole resolution cell. In this study, we assume a beamwidth of 30°, which is a typical value for GNSS-R receivers. Moreover, we consider the signal scattered from only one of the two ambiguous cells. This might be viable, for example, by properly pointing the receiving antenna beamwidth.

Fig. 2 and Fig. 3 show the SNR of the sea surface return received by an airborne and a spaceborne receiver, respectively, as a function of the zenith scattering angle ϑ_s for both right (R) and left (L) circular polarization channels and for different sea states (low, moderate, and high) and azimuth scattering angles φ_s. Additionally, results obtained via GO are shown as well. We assume a viewing angle $\vartheta = 15°$, and wind direction $\varphi_w = 0°$.

As it is expected, the SNR peak in RL is measured in the conventional forward-scattering configuration as, in that direction, both the sea surface NRCS and the resolution cell area exhibit their largest value. It is worth noting that in acquisition geometries close to the conventional one, the GO contribution dominates and, hence, using BA-PTSM does not offer an appreciable advantage. When moving far from the specular reflection direction, GO attenuates much faster than BA-PTSM and severely underestimates the received signal strength. The deviation from BA-PTSM increases with decreasing wind speed and increasing φ_s. Additionally, GO offers poor accuracy for the evaluation of the RR channel in backscattering where it predicts a deep SNR fall, which is absent in BA-PTSM results.

Finally, it is worth noting that a reliable simulation of sea-reflected GNSS signals using standard receivers and processing does not call for scattering models more accurate than GO at any acquisition geometry and sea state. Indeed, at spaceborne altitudes, GO is accurate for acceptable SNR values. Conversely, the adoption of a more accurate scattering model, e.g., BA-PTSM, is of key relevance for airborne GNSS-R, even assuming conventional receivers, such as GOLD-RTR.

5 Conclusion

In this paper, we carried out an analysis of the SNR of the sea surface returns received by spaceborne and airborne GNSS-R receivers in acquisition geometries other than the conventional forward-scattering one. Such an analysis might be fruitfully exploited for a reliable simulation of GNSS signals in arbitrary acquisition geometries as it is required, for example, in maritime surveillance applications. For an accurate and fast evaluation of sea surface scattering at arbitrary viewing geometries we relied on a recent bistatic two-scale scattering model for anisotropic rough surfaces, named BA-PTSM.

Numerical results comparing BA-PTSM with GO have shown that the simulation of airborne GNSS signals scattered off sea surface requires a scattering model more accurate than GO if acquisition geometries other than the conventional forward-scattering one are of interest, e.g., in maritime surveillance applications. This has been demonstrated even assuming a standard GNSS-R receiver, such as GOLD-RTR. Conversely, GO offered enough accuracy in the spaceborne scenario regardless of the sea state, at least assuming conventional receivers, as in this case SNR is larger than 0 dB only in a much narrower range of acquisition geometries.

6 References

1. V. U. Zavorotny, S. Gleason, E. Cardellach, and A. Camps, “Tutorial on remote sensing using GNSS bistatic radar of opportunity,” *IEEE Geoscience and Remote Sensing Magazine*, **2**, 4, 2014, pp. 8–45.

2. A. Di Simone, *et al.*, “Sea target detection using spaceborne GNSS-R delay-Doppler maps: Theory and experimental proof of concept using TDS-1 data,” *IEEE J. Sel. Topics Appl. Earth Observ. Remote Sens.*, **10**, 9, 2017, pp. 4237–4255.

3. A. Di Simone, A. Iodice, D. Riccio, A. Camps, and H. Park, “GNSS-R: A useful tool for sea target detection in near real-time,” *2017 IEEE 3rd International Forum on Research and Technologies for Society and Industry (RTSI)*, 2017, pp. 1–6.

4. A. Di Simone, P. Braca, L. M. Millefiori and P. Willett, "Ship detection using GNSS-reflectometry in backscattering configuration," *2018 IEEE Radar Conference (RadarConf18)*, Oklahoma City, OK, 2018, pp. 1589-1593.

5. B. J. Southwell, J. W. Cheong and A. G. Dempster, "A Matched Filter for Spaceborne GNSS-R Based Sea-Target Detection," *IEEE Trans. Geosci. Remote Sens.*, **58**, 8, Aug. 2020, pp. 5922-5931.

6. M. Clarizia, *et al.*, "Target detection using GPS signals of opportunity," *2015 18th International Conference on Information Fusion*, Washington, DC, 2015, pp. 1429-1436.

7. T. Beltramonte, *et al.*, "Simulation-Based Feasibility Analysis of Ship Detection Using GNSS-R Delay-Doppler Maps," *IEEE J. Sel. Topics Appl. Earth Observ. Remote Sens.*, **13**, 2020, pp. 1385-1399.

8. G. Di Martino, A. Di Simone, A. Iodice and D. Riccio, "Bistatic Scattering From Anisotropic Rough Surfaces via a Closed-Form Two-Scale Model," *IEEE Trans. Geosci. Remote Sens.*, doi: 10.1109/TGRS.2020.3021784.

9. A. Iodice, A. Natale, and D. Riccio, "Retrieval of Soil Surface Parameters via a Polarimetric Two-Scale Model", *IEEE Trans. Geosc. Remote Sens.*, **49**, 7, July 2011, pp. 2531-2547.

10. G. R. Valenzuela, "Scattering of Electromagnetic Waves from a Tilted Slightly Rough Surface", *Radio Sci.*, **3**, 1968, pp. 1057-1066.

11. G. Di Martino, A. Iodice, D. Riccio, "Closed-Form Anisotropic Polarimetric Two-Scale Model for Fast Evaluation of Sea Surface Backscattering", *IEEE Trans. Geosc. Remote Sens.*, **57**, 8, 2019, pp. 6182-6194.

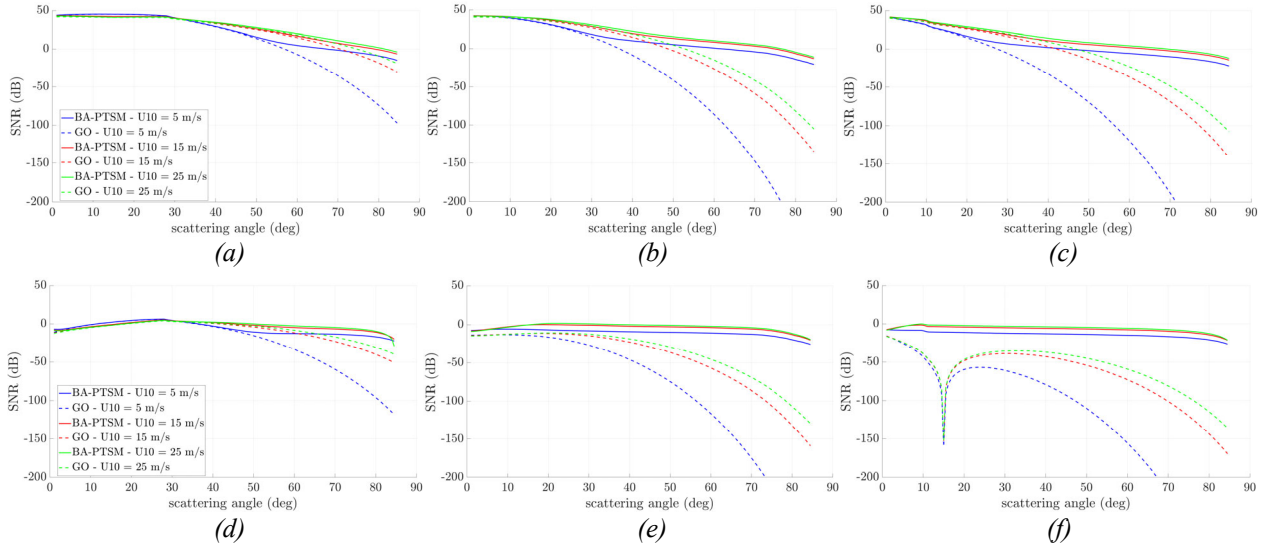

Figure 2: SNR as a function of the zenith scattering angle ϑ_s in RL (a-c) and RR (d-f) for an airborne GNSS-R receiver (GOLD-RTR) assuming wind speed U_{10} = 5 m/s (blue lines), 15 m/s (red lines), and 25 m/s (green lines). Viewing angle is ϑ = 15°, wind direction is the positive *x*-axis. BA-PTSM (solid lines) is compared with GO (dashed lines). (a, d) φ_s = 0°; (b, e) φ_s = 90°; (c, f) φ_s = 180°.

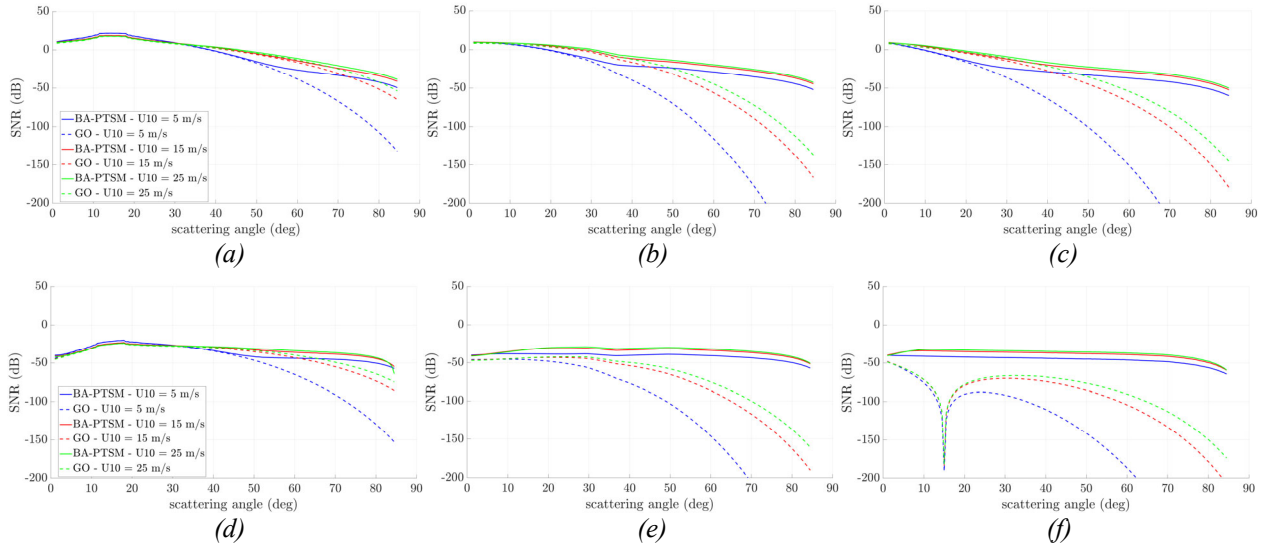

Figure 3: SNR as a function of the zenith scattering angle ϑ_s in RL (a-c) and RR (d-f) for a spaceborne GNSS-R receiver (SGR-ReSi) assuming wind speed U_{10} = 5 m/s (blue lines), 15 m/s (red lines), and 25 m/s (green lines). Viewing angle is ϑ = 15°, wind direction is the positive *x*-axis. BA-PTSM (solid lines) is compared with GO (dashed lines). (a, d) φ_s = 0°; (b, e) φ_s = 90°; (c, f) φ_s = 180°.